scientific reports

Check for updates

OPEN

Optimization of amorphous silicon solar cells through photonic crystals for enhanced optical properties

Hassan Sayed[1]✉, Ashour M. Ahmed[2], Ali Hajjiah[3], M. A. Abdelkawy[4] & Arafa H. Aly[1]

Amorphous silicon solar cells have emerged as a promising technology for harnessing solar energy due to their cost-effectiveness and flexibility. However, their efficiency is constrained by low sunlight absorption resulting from the material's indirect band gap and intrinsic properties of amorphous silicon. This study employs theoretical modeling to investigate the impact of incorporating one-dimensional ternary photonic crystals (1D-Ternary-PCs) as anti-reflection coatings (ARCs) and one-dimensional binary PCs as back reflectors to enhance the optical properties of amorphous silicon (a-Si) solar cells. The investigation utilizes the COMSOL Multiphysics program, based on the finite element method (FEM), to simulate and analyze the optical characteristics of PC-enhanced a-Si solar cells. The modeling involves designing and optimizing ternary PC structures, followed by numerical simulations to assess their anti-reflection performance. Additionally, designing one-dimensional binary PCs optimized to create a photonic band gap within the transmitted spectrum to act as a back reflector. The study systematically examines the impact of various parameters such as layer thickness, refractive indices, and incident angles on the optical properties of PC-enhanced a-Si solar cells, offering insights into the potential of one-dimensional PCs as effective back reflectors and ARCs for enhancing light absorbance and overall efficiency.

Keywords Amorphous silicon solar cells, Photonic crystals, Anti-reflection coatings (ARCs), COMSOL multiphysics

The world is currently facing an energy crisis and climate change due to the rapidly growing demand for energy and the finite supply of non-renewable sources such as fossil fuels[1]. This has led to the search for alternative, sustainable, and ecologically acceptable energy sources[2,3]. Solar energy is a type of renewable energy that can be captured using solar cells. Solar cells convert sunshine into power, making them an attractive solution to the energy crisis[4,5]. Solar energy is a renewable energy source that is plentiful and readily accessible. According to the International Energy Agency (IEA), solar energy is predicted to be the greatest source of power by 2050, accounting for approximately 37% of the world's electricity generation[7]. Solar cells have come a long way since their invention in the 1950s and are now highly efficient and cost-effective. The cost of solar energy has decreased significantly over the past decade and is now cheaper than fossil fuels in many parts of the world[8–10].

The growing desire for clean and sustainable energy sources has resulted in considerable advances in photovoltaic (PV) technology. Among these, amorphous silicon (a-Si) solar cells have attracted considerable interest owing to their low-cost fabrication processes[11–13], compatibility with flexible substrates, and potential for large-scale production. However, a-Si solar cells have a limited ability to absorb sunlight efficiently, which restricts their overall conversion efficiency[14,15]. Thus, one promising approach to improve the solar cell absorbance is the incorporation of photonic crystals (PCs)[16,17]. PCs are periodic structures with a unique refractive index distribution that can manipulate the propagation of light by controlling its dispersion and reflectance properties[18–20]. By carefully designing and engineering the PCs structures, it is possible to enhance light trapping inside the active area of the solar cell, thereby increasing the probability of photon absorbance[21].

[1]Physics Department, Faculty of Sciences, TH-PPM Group, Beni-Suef University, Beni Suef 62514, Egypt. [2]Physics Department, College of Science, Imam Mohammad Ibn Saud Islamic University (IMSIU), Riyadh 11623, Saudi Arabia. [3]Electrical Engineering Department, College of Engineering and Petroleum, Kuwait University, Kuwait City, Kuwait. [4]Department of Mathematics and Statistics, College of Science, Imam Mohammad Ibn Saud Islamic University (IMSIU), Riyadh 11432, Saudi Arabia. ✉email: hassansayed@science.bsu.edu.eg

Numerous studies have demonstrated the potential of photonic crystals (PCs) to advance the performance of many solar cell technologies, including thin-film, crystalline silicon and Dye-sensitized solar cells[22–25]. However, the application of PCs in amorphous silicon solar cells is still at an early stage, with limited research exploring their full potential[26]. For instance, Li et al. (2014) investigated the efficiency enhancement of amorphous silicon solar cells using photonic crystal configurations[14]. Similarly, Lin et al. (2015) focused on the design and fabrication of photonic crystal structures to improve light trapping in amorphous silicon solar cells[27]. Zhang et al. (2016) explored the utilization of photonic crystal nanostructures to enhance light trapping in amorphous silicon solar cells as well[28]. Additionally, Chutinan et al. (2005) optimized photonic crystal light-trapping in thin-film solar cells[29], while Zhang et al. (2014) studied the design and optimization of photonic crystal structures for enhanced light trapping in amorphous silicon thin film solar cells[30]. These studies collectively demonstrate the potential of photonic crystals in improving the performance of various solar cell technologies. Therefore, this paper purposes to address this research gap by examining the effects of integrating photonic crystals into amorphous silicon solar cells to enhance their optical properties. Wherein we intended to use the photonic crystals as an anti-reflection coating (ARC) and back reflector to the amorphous silicon solar cell to overcome the power dissipation by reflection and transmission.

The usage of photonic crystals (PCs) as an anti-reflection coating (ARC) and back reflector to the amorphous silicon solar cell has been extensively explored in research. For instance, Zhang et al. (2012) investigated the application of a one-dimensional photonic crystal as an anti-reflection coating to improve the silicon solar cells absorbance[31]. Similarly, Jeong et al. (2014) proposed a photonic crystal structure as a back reflector to improve the light trapping and absorption in amorphous silicon solar cells[32]. Furthermore, Wang et al. (2017) studied the design and optimization of photonic crystal structures as both the back reflector and anti-reflection coating for amorphous silicon solar cells[33]. These studies highlight the potential of photonic crystals in serving dual roles, providing effective anti-reflection properties and enhancing light trapping as back reflectors in amorphous silicon solar cells.

In this paper, we try to limit the energy dissipation in solar cells by each of reflection from the top surface and transmission from the lower surface of the cell by using different structures from 1D-PCs. The rest of the paper is arranged as follows: Sect. "Modeling" gives a thorough description of the theoretical background and prior research on photonic crystals and their applications in solar cells, including the construction of photonic crystal structures. Section "Results and discussions" introduces and discusses the optical characteristics and device performance of the amorphous silicon solar cells combined with photonic crystals. Finally, we discuss the implications of the findings, highlight the potential challenges, and propose future directions for further research.

Modeling

This section describes the design and optimization process of photonic crystal structures for integration into a-Si solar cells. It explains the selection of relevant parameters, such as layer thicknesses, refractive index contrast, and structural configuration, and discusses the design considerations for achieving optimal light trapping and absorption enhancement. The numerical simulation methodology using COMSOL Multiphysics program is detailed in this section. It includes the finite element method (FEM) simulations procedure as the simulation technique employed to analyze the optical characteristics of the PC-enhanced a-Si solar cells[34,35].

We chose the FEM implemented in COMSOL Multiphysics Because of its capacity to achieve complicated geometries, curved interfaces, and layered structures with subwavelength features—all of which are essential components of our amorphous silicon solar cell with multilayer ARC and back reflector—. For non-periodic, non-uniform, and radially symmetric structures like the ones we employ in our study, FEM provides great accuracy in solving Maxwell's equations in complete vectorial form. FEM offers the best trade-off for geometry adaptability, meshing flexibility, and field visualization at numerous wavelengths, whereas techniques like Transfer Matrix Method (TMM) or Rigorous Coupled-Wave Analysis (RCWA) are effective for periodic, planar structures and Finite-Difference Time-Domain (FDTD) is strong for broadband simulations. This made it possible for us to accurately record optical responses and field localization, which were essential for our cell's design and optimization. In our study, we adopted a mesh refinement strategy based on the shortest operating wavelength, ensuring that the maximum mesh element size was no larger than $\lambda/10$, where λ is the shortest wavelength of interest (300 nm). Additionally, we applied extra fine meshing at material interfaces and within the a-Si intrinsic region, where field localization is most critical.

Our design is divided into two parts: firstly, we describe the design and optimization process of one-dimensional ternary PC structures for integration as ARCs in a-Si solar cells. It explains the selection of relevant parameters, such as layer thickness and refractive indices, and discusses the design considerations for achieving optimal anti-reflection properties. Then, we Design one-dimensional PCs as a back reflector for amorphous silicon (a-Si) solar cells involves tailoring the PC structure to maximize light trapping and reflection within the device. The design process typically focuses on optimizing parameters such as the periodicity, refractive index contrast, and layer thickness to achieve enhanced light management[37]. By carefully engineering the PC structure, the desired photonic bandgap can be achieved[36], which facilitates the efficient reflection and redirection of incident light back into the a-Si active layer. The selection of materials and their thicknesses within the PC layers is crucial in determining the reflection characteristics and overall optical performance. The successful design of one-dimensional PCs as back reflectors holds significant promise for enhancing the light trapping and absorption properties of a-Si solar cells, thereby improving their overall efficiency.

Our structure is made up of a p-region with a thickness of 15 nm, an intrinsic area with a thickness of 200 nm, and an n-region with a thickness of 27 nm. Whereas figure 1 depicts our model when ARC and back reflector are present. Here, ARC have different structures –Single layer, binary, ternary PCs- with step index between the air and silicon layer as following;

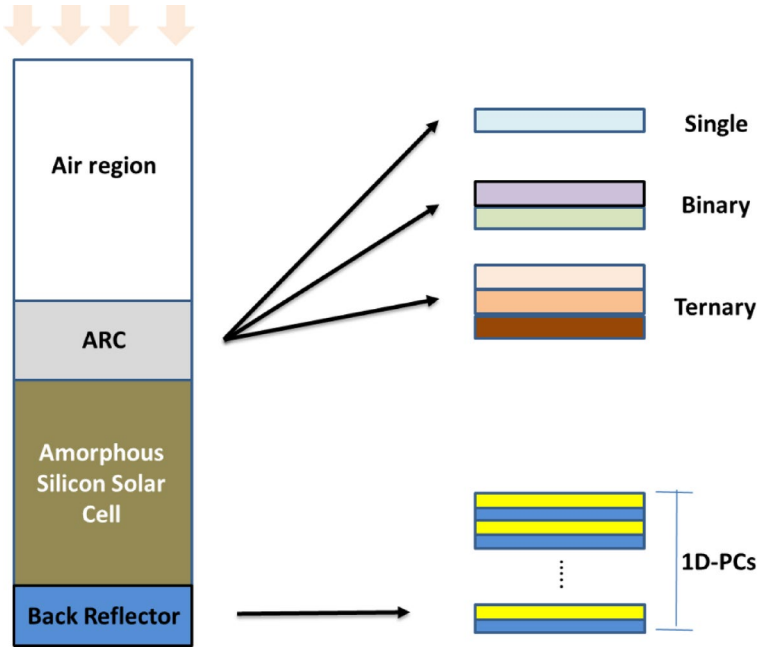

Fig. 1. Schematic representation of our design, showcasing an amorphous silicon solar cell positioned between the antireflective coating and the back reflector.

$$n_{air} < n_{ARC} < n_{a-Si}$$

Also, the back reflector is composed of 1D binary PCs (two layers with different dielectric constant), 1D-PCs is optimized to create PBG in the range of the transmitted spectrum to contribution in the generation rate of electron hole pair to increase the overall efficiency.

The optical simulations are based on wavelength-dependent complex refractive indices $(n + i\,k)$for each material. Therefore, we provide graphs showing the dispersion curves (real and imaginary parts) of refractive indices. Wherein, the response of the real and imaginary parts of the amorphous silicon (a-Si), which is regarded as the active area of the cell, to the incident wavelength is shown in Figure 2. In this case, the real part of the dielectric constant (refractive index) increases with wavelength to reach 5.0 at about 450 nm, after which it starts to decrease to equal 4.0 at 800 nm. Additionally, the imaginary part of the dielectric constant (extinction coefficient) decreases with wavelength increments to reach very small values close to zero at the end of the visible region. A comparatively good compatibility with these findings is examined in Fig. 2 [39,40]. In this case, the absorption values within the cell may be affected differently by the values of the real and imaginary components.

Figure 3 shows the dispersion relation of the refractive index (n) as a function of wavelength for magnesium fluoride (MgF_2), the refractive index decreases with increasing wavelength, which is a characteristic of normal dispersion. This means that the material becomes less optically dense (lower refractive index) at longer wavelengths. As the wavelength increases beyond ~700 nm, the change in the refractive index becomes smaller, indicating the material's dispersion becomes weaker in the near-infrared range[40]. In addition, the extinction coefficient of MgF_2 is relatively to zero as the material is a dielectric with zero absorption in the visible spectrum range. When creating photonic structures and anti-reflective coatings (ARCs), this type of dispersion profile is essential. It controls how light is coupled or reflected at interfaces in solar cells, particularly in wavelength ranges between 300 and 800 nm that are crucial for solar spectrum absorption.

The complex refractive index for silicon nitride (Si_3N_4) which considered as well-characterized substance, may be found on refractiveindex.info[42]. SiN_x, on the other hand, refers to silicon nitride films with different stoichiometry, where the value of 'x' may change depending on the circumstances of deposition. It is difficult to give a single, standardized dispersion relation for SiN_x because of this diversity, which results in variations in optical characteristics. According to studies, the composition and deposition technique of SiN_x films can have a substantial impact on their refractive index[41]. Also, Microcrystalline Hydrogenated Silicon Dioxide ($\mu\,c - SiO_2 : H$) is a specialized material with limited availability of optical data. Its complex refractive index can vary based on factors such as hydrogen content and microcrystalline structure[42].

Results and discussions

Here, we show our results and discuss them over four main steps: Initially, we study the optical properties of an a-Si solar cell to compute the main reasons for the low optical absorbance, and then we try to design an optimum anti-reflection coating with step index criteria to achieve low reflection from the upper layer of the cell. In the third step, we design a back mirror from a 1D Bragg reflector to minimize the transmitted photons. Finally, we calculate the generation rate of electron hole pairs owing to the optical absorbance.

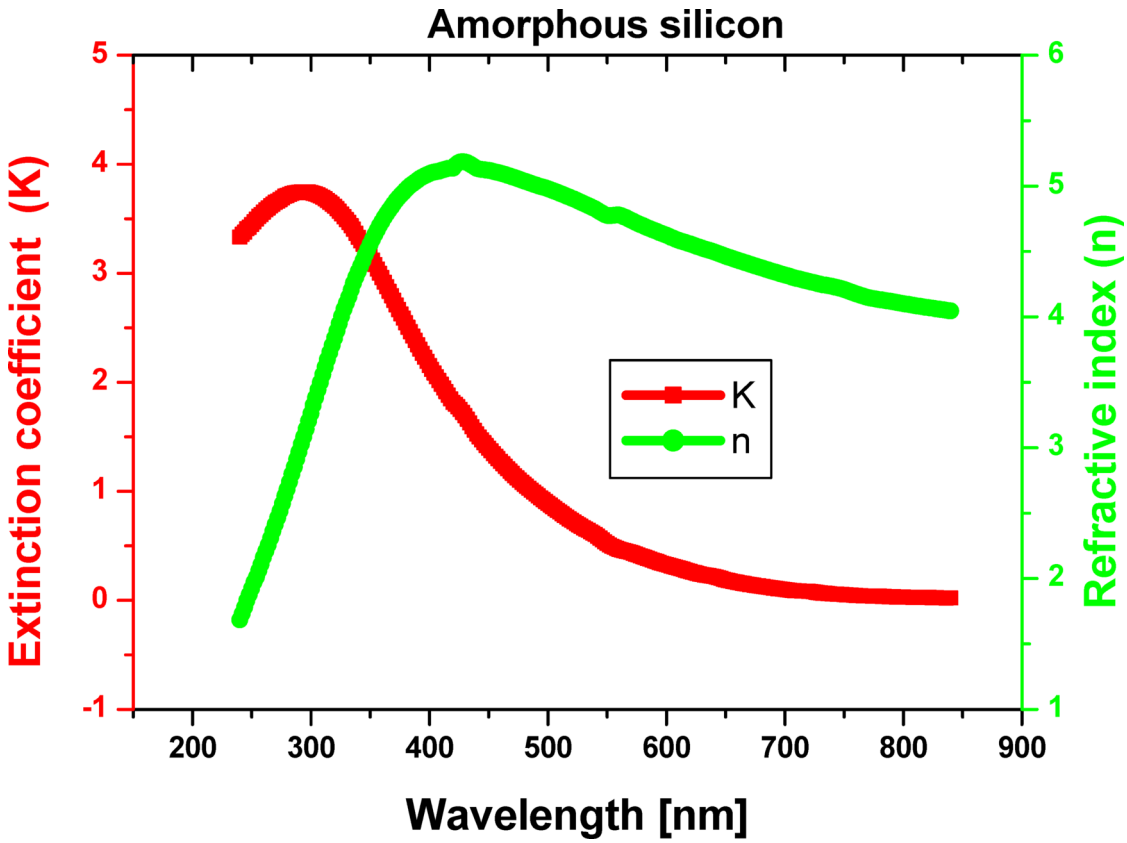

Fig. 2. Refractive index and extinction coefficient of amorphous silicon as a function of the wavelength of the incident radiation.

Optical properties of an amorphous silicon solar cell

In this study, we propose a PIN silicon solar cell featuring specific layer thicknesses: a p-region measuring 15 nm, an intrinsic region of 200 nm, and an n-region that is 27 nm thick. Then, we calculate the optical properties of the cell such as absorbance (A), transmission (T), and reflection (R) as we shown in Fig. 4. Fig. 4 is representing A, T, and R of an a-Si solar cell with an energy gap equal to 1.7 eV. The reflectance (red line) is approximately equals 40% from the incident photons because of the reflectance of the amorphous silicon is equivalent to 37% as we discussed previously in the introduction part, Also, the transmittance (green line) is considered to begin at 550 nm as in the figure, hence, the maximum absorbance of the cell is reached to 55% at the incidence of wavelength equals 550 nm. The inherent optical characteristics of amorphous silicon, its indirect bandgap (~ 1.7 eV) and the optimized selected thickness for each layers are responsible for the peak seen in the absorption spectrum close to 550 nm. Strong absorption occurs at this wavelength because photons have enough energy to activate electrons across the bandgap. The troughs that lie next to this peak are brought on by the thin active layer's restricted absorption depth, mismatched impedance at the interfaces, and enhanced reflection and partial transmission. The electric field distribution in Fig. 5B, which maximizes photon absorption within the cell by efficiently penetrating the intrinsic area at 550 nm, supports this.

Hence, we compute the electric field distribution inside the layers of the cell for different incident wavelengths as we shown in Fig. 5. For $\lambda = 300\,nm$, the incident wave is completely absorbed in few nanometers from the top surface of the cell, for $\lambda = 550\,nm$, the electric field is distributed over a wide thickness of the cell as we shown in Fig. 5B without any transmitted photons. Also, for $\lambda = 800\,nm$, the penetration depth of the incident photon is increased as shown in Fig. 5C with respect to Fig. 5B and the cell will be transparent for any photons greater than these photons owing to its energy gap. Hereby, to enhance the optical properties of the cell, we need to eliminate the last shortcomings of reflection and transmission. Hence, we need to design anti-reflection coating (ARC) to override the reflectance, and design back mirror to eliminate the transmittance of the cell. Therefore, in the next sub-sections we design and optimize each of ARC and back reflector, respectively.

Anti-reflection coating

ARC is an intermediate layer between the first layer of the cell and air, which verify the step index of the refractive indices. The optimum ARC structure is characterized by achieving low reflectivity and high transmittance. This section is divided to three sub-sections [Single, binary, and ternary] corresponding to the number of layers in each ARC structure as we show in Table 1, since complete wavelength-dependent dispersion data was utilized in the actual simulations, these numbers are just given for illustrative purposes.

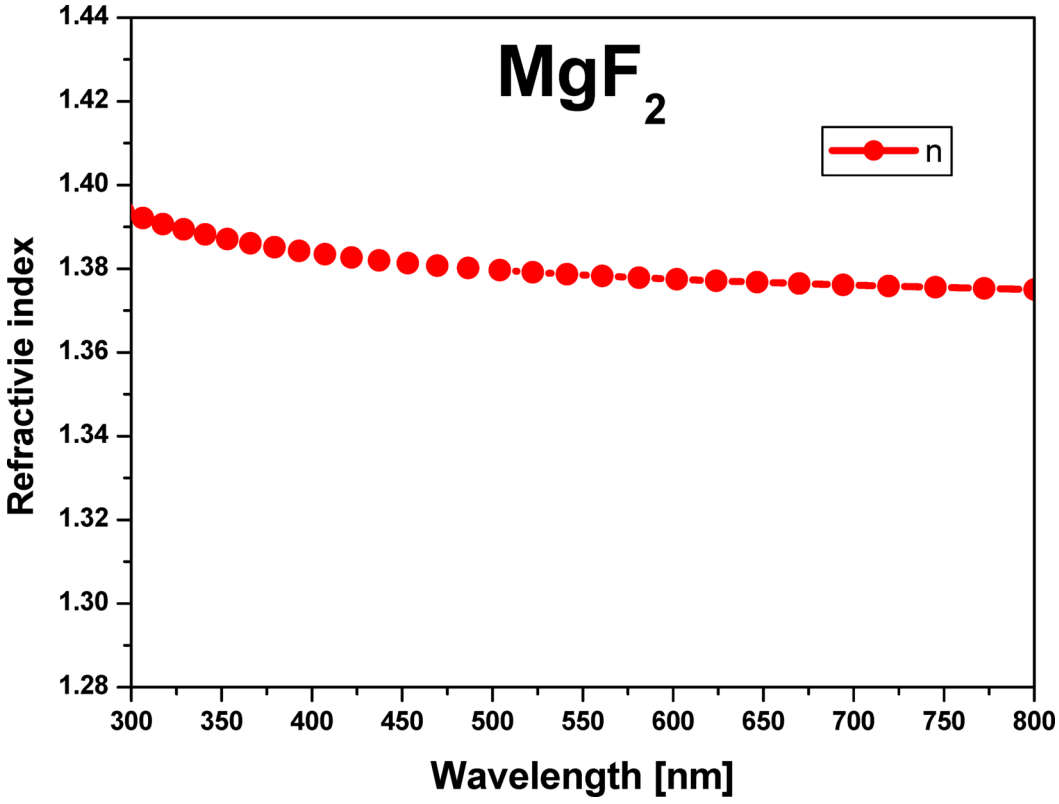

Fig. 3. Refractive index of Magnesium Fluoride (MgF_2) as a function of the incident wavelength.

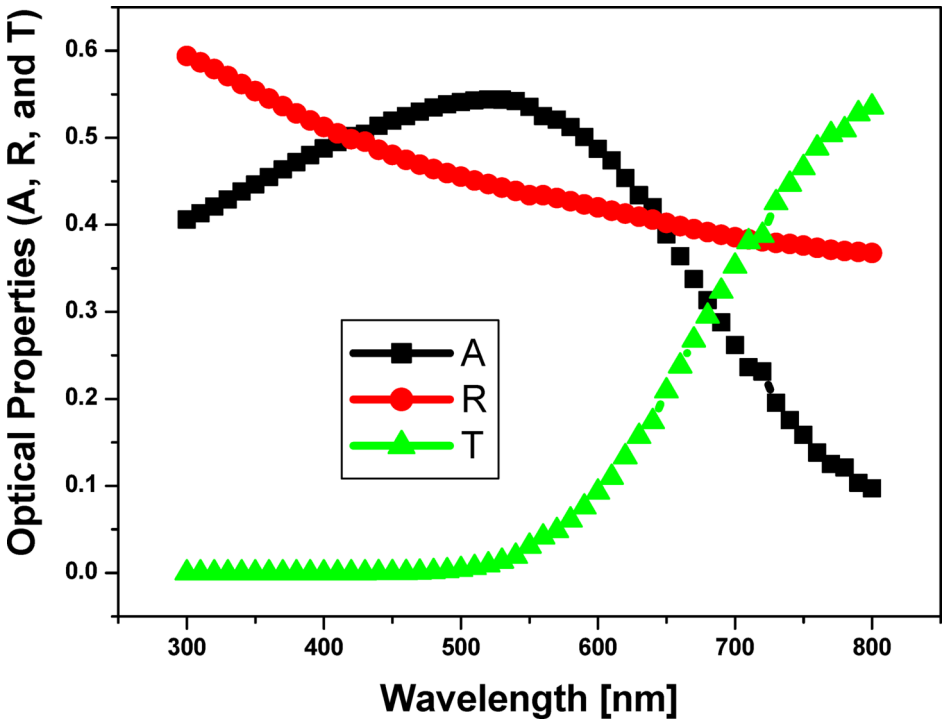

Fig. 4. Transmission, absorption, and reflection of amorphous silicon solar cell as a function of incident wavelength.

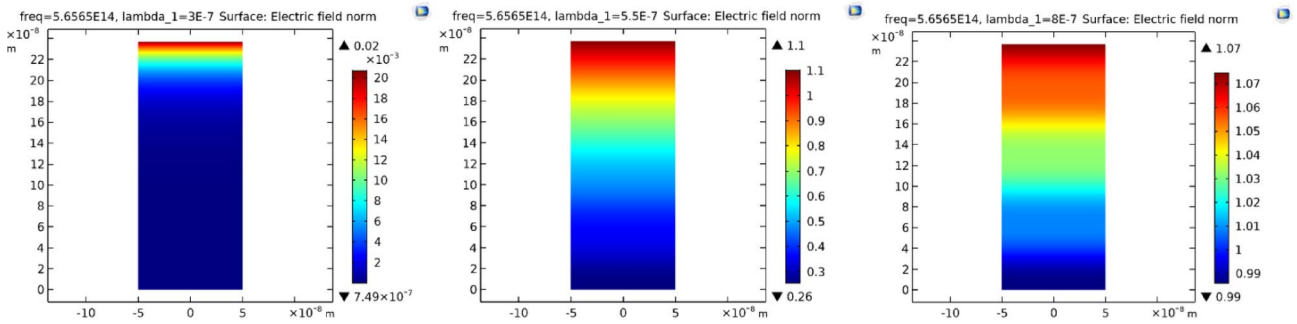

Fig. 5. The electric field distribution through the active layer of the cell at different incident wavelengths (**a**) $\lambda = 300\,nm$, (**b**) $\lambda = 550\,nm$, and (**c**) $\lambda = 800\,nm$.

Planner					
Single	Binary		Ternary		
SiN_x[38]	TiO_2[44]	SiO_2[43]	$\mu c - SiO_x : H$[46]	SiN_x	MgF_2[45]
$n_1 = 1.92$ $d_1 = 60\,nm$	$n_1 = 2.5$ $d_1 = 40\,nm$	$n_2 = 1.46$ $d_2 = 80\,nm$	$n_1 = 2.8$ $d_1 = 50\,nm$	$n_2 = 1.96$ $d_2 = 50\,nm$	$n_3 = 1.38$ $d_3 = 50\,nm$

Table 1. Different planner ARC structures with each layer's nominal thickness and refractive index.

Single layer ARC

We examined the best refractive index for a single ARC layer between air and silicon according to $n_1 = \sqrt{(n_0 n_s)}$ since n_0, n_s *and* n_1 are the refractive indexes of air, silicon wafer, and anti-reflection coating single layer. Thus, it is thought that the best material for use in the ARC is SiN_x with a refractive index equals 1.92 which could be manufacturing by using spray pyrolysis techniques. Therefore, we optimize the thickness of this single layer acting as ARC to verify high transmittance as shown in Fig. 6. In Fig. 6, adding SiN_x is achieved the step index, thus, SiN_x is enhance the cell absorbance overall, increasing the thickness of SiN_x from 50 nm to 60 nm cause an enhancement in the cell absorbance, then any increase over 60 nm cause decreasing in the absorbance. Therefore, the best thickness for this material to act as ARC is 60 nm as in the Fig. 6.

Binary ARC

Here, we design a binary structure (two layers from different dielectric materials) and optimize the thickness of each layer as shown in Fig. 7. In Fig. 7A, adding a binary ARC composed of SiO_2, and TiO_2 with refractive indices $n_1 = 1.46$, $n_2 = 2.5$, respectively, increases the absorbance with respect to the cell without ARC. In Fig. 7A, we study the effect of TiO_2 thickness at the thickness of SiO_2 equal to 100 nm, wherein, by increasing the thickness, the absorbance also increases up until the thickness reaches 80 nm; therefore, the best thickness of TiO_2 is 80 nm. Thus, in Fig. 7B, we study the effect of SiO_2 thickness at the thickness of TiO_2 equal to 80 nm, beginning with $d_1 = 20\,nm$, and $d_2 = 80\,nm$ and increasing the value of d_1 from 20 nm to 40 nm has a positive effect on the cell absorbance. Then, any increase in the value of d_2 causes a decrease in the absorbance as shown in Fig. 7B. Hence, we found that the best thicknesses for the binary structure, which is composed of SiO_2, and TiO_2 are 40 nm and 80 nm, respectively.

Ternary ARC

The one-dimensional ternary PC structure is composed of three layers of different dielectric materials. Here, we design and optimize the considered structure to achieve a step index and minimize cell reflectivity. Therefore, we choose the three materials as MgF_2, SiN_x , and $\mu c - SiO_x : H$, with refractive indices donated by $n_1 = 1.38$, $n_2 = 1.96$ and $n_3 = 2.8$, respectively, which achieve the step index between the air and silicon layer. Thus, we optimize the thickness of each layer as shown in Fig. 8 because adding a ternary ARC composed MgF_2, SiN_x , and $\mu c - SiO_x : H$ increases the absorbance with respect to the cell without ARC.

In Fig. 8A, we study the effect of MgF_2 thickness at the thicknesses of SiN_x , and $\mu c - SiO_x : H$ donated by $d_2 = 33\,nm$, $d_3 = 54\,nm$. Wherein, by increasing the thickness, the absorbance also increases up until the thickness reaches 20 nm; therefore, the best thickness of MgF_2 is 20 nm. Thus, in Fig. 8B, we study the effect of SiN_x thickness at the thickness of MgF_2, and $\mu c - SiO_x : H$ donated by $d_1 = 20\,nm$, $d_3 = 54\,nm$, wherein, by increasing the thickness, the absorbance also increases up until the thickness reaches 20 nm; therefore, the best thickness of SiN_x is 20 nm. In Fig. 8C, we optimize the thickness of $\mu c - SiO_x : H$ layer at the thickness of MgF_2, and SiN_x donated by $d_1 = 20\,nm$, $d_2 = 20\,nm$, changing the value of d_3 from 20 nm to 54 nm has a positive effect on the cell absorbance. Then, any increase in the value of d_3 causes

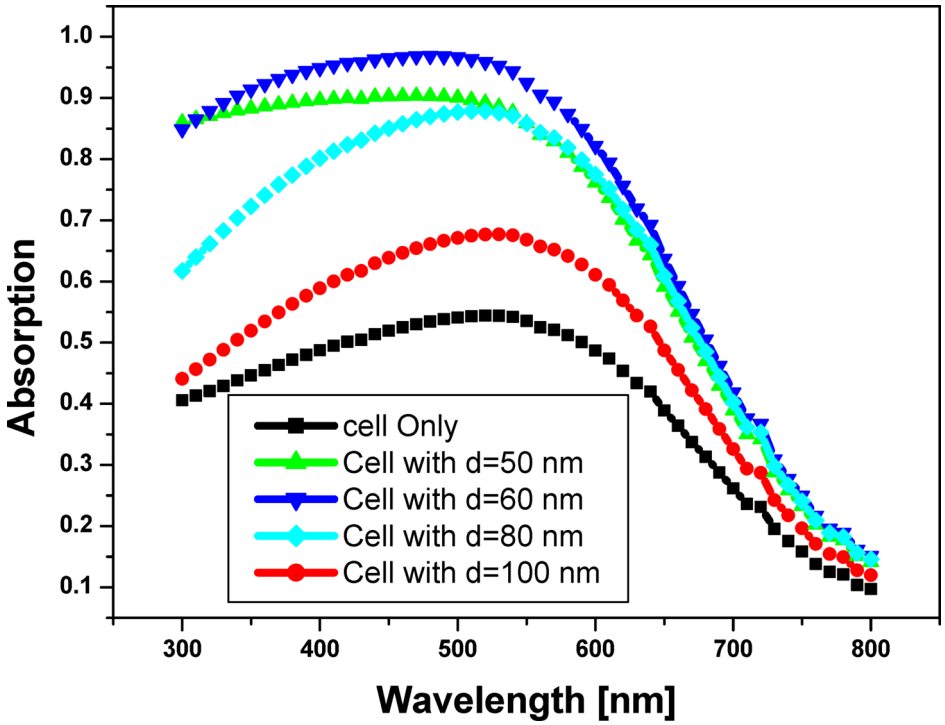

Fig. 6. Absorption of amorphous silicon solar cell by adding a single layer from SiN_x with different thickness as a function of incident wavelength as shown.

a decrease in the absorbance, as shown in Fig. 8C. Hence, we found that the best thicknesses for the ternary structure, which is composed MgF_2, SiN_x , and $\mu c - SiO_x : H$, are 20 nm, 20 nm and 54 nm, respectively.

At the end of this section, we compare the optimized structures for each case from the last three cases (single layer, binary structure, and ternary structure), as shown in Fig. 9. Figure 9 represents the absorption spectrum for amorphous silicon (a- Si) solar cell by adding ARC with different structures. The single layer is composed of an only one layer of $SiN_x$with thickness of 60 nm. Binary is composed of TiO_2 with a thickness equal to 40 nm and SiO_2 with a thickness equal to 80 nm. Ternary is composed of MgF_2, SiN_x , and $\mu c - SiO_x : H$, where ; $d_1 = 20\,nm$, $d_2 = 20\,nm$, and $d_3 = 54\,nm$, respectively. In Fig. 9, all three cases have a positive effect on the cell absorbance for the incident photons wavelengths from 300 nm to 550 nm, but the ternary optimize construction is more effective for this range of wavelengths in the enhancement of the cell absorbance, as shown. Therefore, the ternary structure is considered the most compatible arrangement to improve cell absorbance and efficiency. However, the absorbance of the cell is still low for incident wavelengths larger than 550 nm owing to the transmitted spectrum in this range. Therefore, we will add a one-dimensional PC structure as a back reflector to return the transmitted photons in the range of the cell energy gap.

Back reflector (Bragg Reflector)

In this sub-section, we try to overcome the shortcoming of the transmitted spectrum, as we found previously in Fig. 4. So that we will add a back reflector to the optimum structure for the ternary ARC. Here, we design 1D-PCs to performance as a back mirror to the cell; therefore, from the transmittance of the cell, as previously shown in Fig. 4, we need to create a structure with high reflectance for the incident photons wavelengths approximately from 525 nm to 750 nm. Hence, to create a wide PBG, we must use materials with a high contrast in refractive index; therefore, we chose MgF_2 with refractive index $(n_1) = 1.38$, and $\mu c - SiO_x : H$ with refractive index $(n_2) = 2.8$.

Initially, we examined how the number of periods influences the appearance of the photonic bandgap (PBG). Our findings indicated that, in this 1D-PC structure, increasing the number of periods led to the emergence of the PBG. Once the PBG was established, further increases in the structure's periods primarily affected the sharpness of the PBG edges. As illustrated in Fig. 10, with N set to 12, the PBG becomes distinctly visible, spanning from 489 nm to 682 nm, resulting in a width of 193 nm. Additionally, prior to reaching the PBG spectrum, increasing N has minimal impact on the overall position of the PBG, although slight variations in the transmission resonance peaks can be observed. As demonstrated in Fig. 10, which represent the relation between the number of periods and photonic band gap characteristic such as bandwidth and edge steepness. Wherein, increasing the number of Bragg reflector periods leads to enhanced edge steepness of the photonic bandgap due to higher reflectivity, improving spectral selectivity and field confinement. However, it also causes bandgap narrowing, reducing the width of the transmission window around the defect mode. This highlights the need to optimize the number of periods to balance performance with design complexity and fabrication scalability.

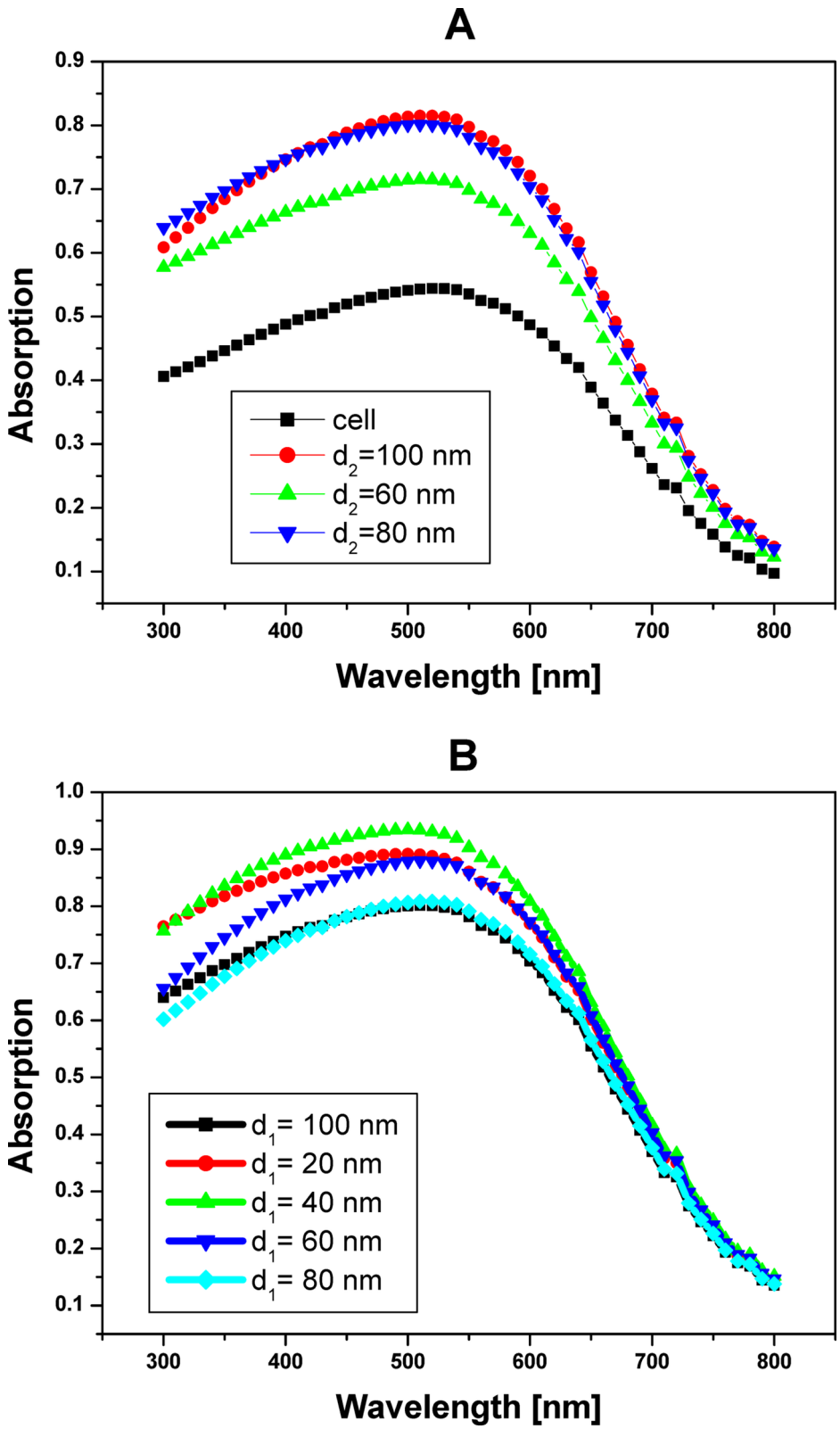

Fig. 7. Absorption of a-Si solar cell by adding a binary ARC, which composed of SiO_2, and TiO_2, where ; (**A**) $d_1 = 100\ nm$ with different values of d_2, (**B**) $d_2 = 80\ nm$ with different values of d_1.

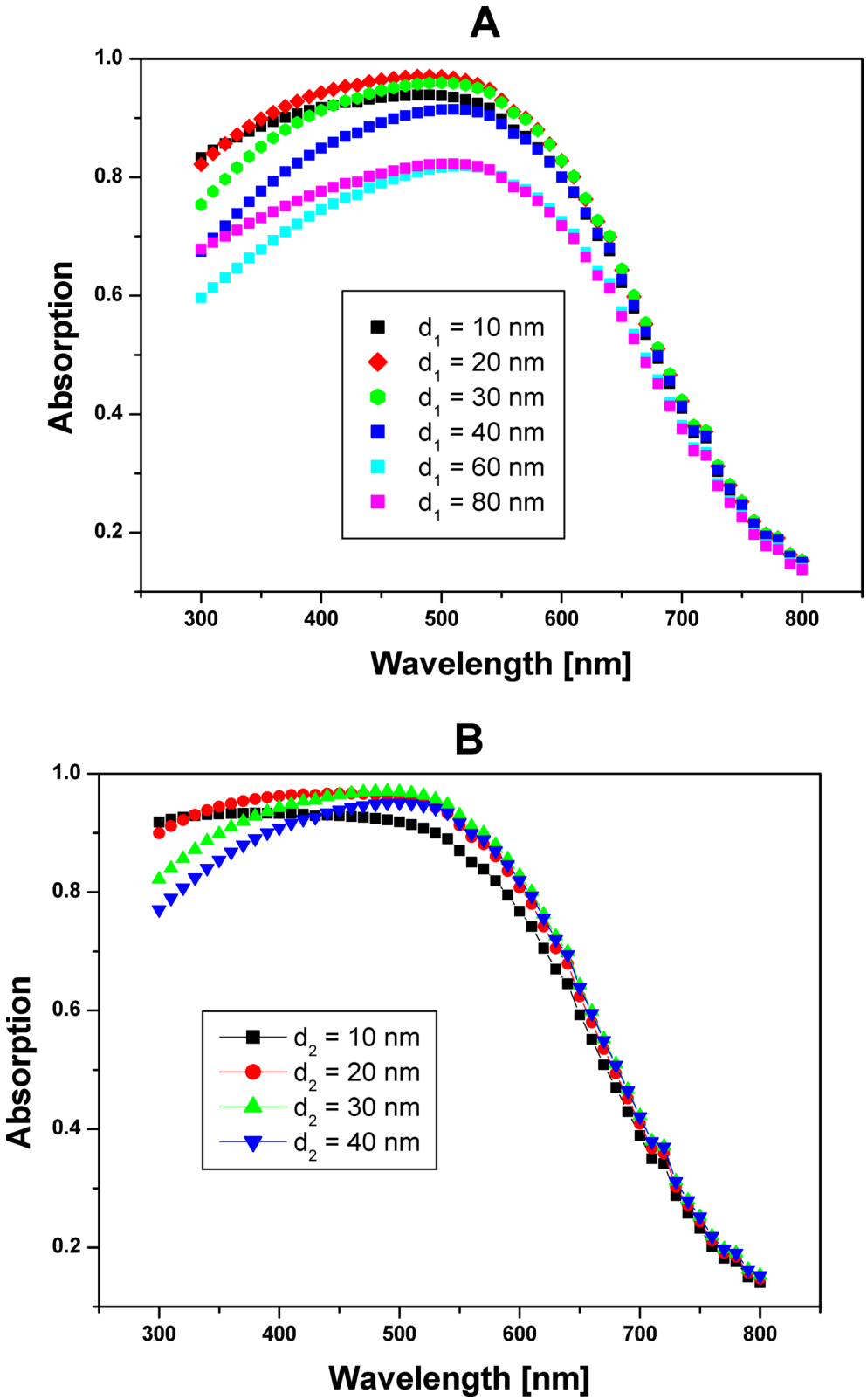

Fig. 8. Absorption of a-Si solar cell by adding a ternary ARC, which composed of MgF_2, SiN_x, and $\mu c - SiO_x : H$, where ; (**A**) $d_2 = 33\,nm$, $d_3 = 54\,nm$ with different thicknesses of the first layer (d_1), (**B**) $d_1 = 20\,nm$, $d_3 = 54\,nm$ with different thicknesses of the second layer (d_2), and (**C**) $d_1 = 20\,nm$, $d_2 = 20\,nm$ with different thicknesses of the third layer (d_3).

When the number of periods is substantially increased, the bandgap narrows while the sharpness of its edges enhances, leading to potential overlaps between the transmittance curves of adjacent bandgaps. This overlap

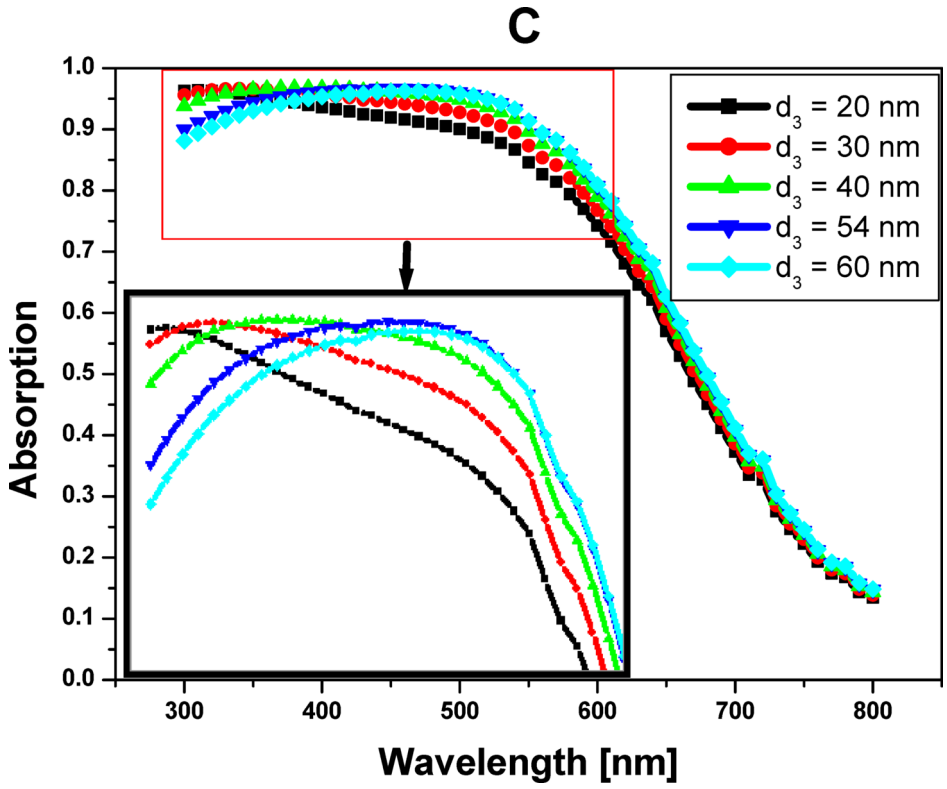

Figure 8. (continued)

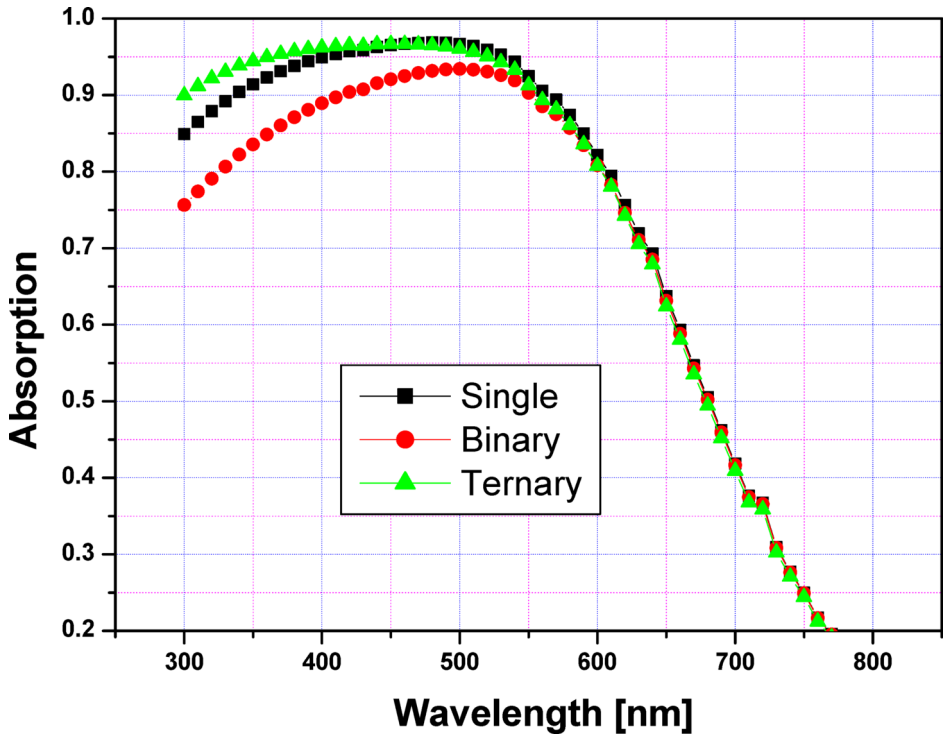

Fig. 9. Absorption of a-Si solar cell by adding ARC with different structures; **Single** is composed of single layer from SiN_x with thickness of 60 nm. **Binary** is composed of TiO_2 with thickness equals to 40 nm, and SiO_2 with thickness equals to 80 nm. **Ternary** is composed of MgF_2, SiN_x, and $\mu c - SiO_x : H$, where ; $d_1 = 20\,nm$, $d_2 = 20\,nm$, and $d_3 = 54\,nm$, respectively.

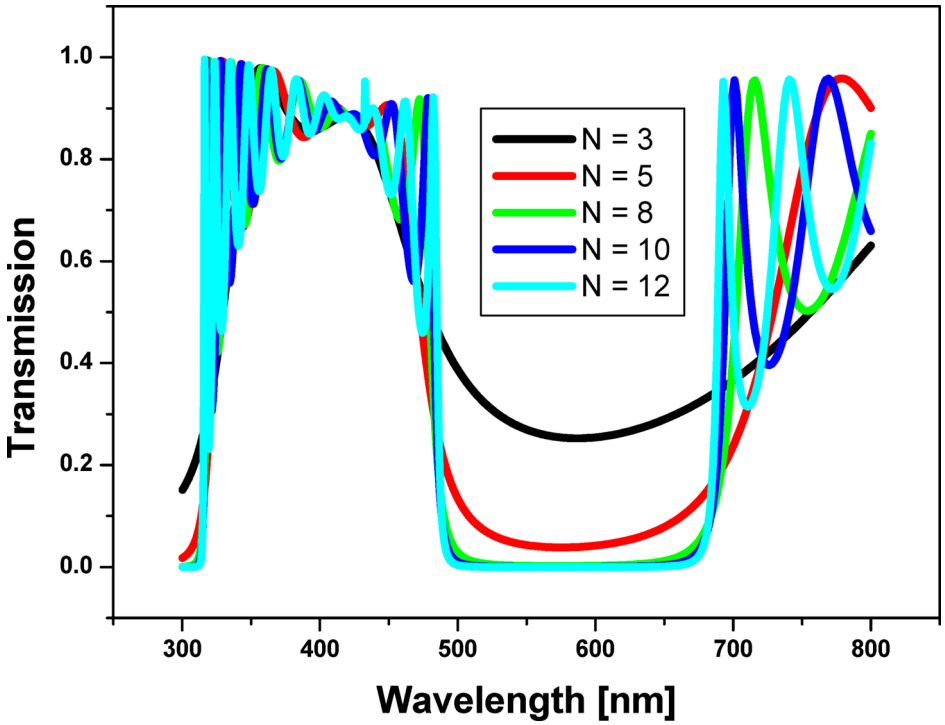

Fig. 10. Transmission spectrum for 1D-PCs which composed of MgF_2 with thickness $(d_1) = 50\,nm$, and $\mu\,c - SiO_x : H$ with thickness $(d_2) = 75\,nm$, with different number of periods as shown.

arises as the bandgaps approach each other in wavelength, causing their transmittance characteristics in those regions to converge. Consequently, the transmittance curves of different bandgaps may either overlap or partially overlap. In summary, augmenting the number of periods in a PBG structure generally results in a narrower bandgap and can facilitate the overlapping of transmittance curves from neighboring bandgaps.

Hence, we investigate the effect of layer thicknesses to localize the PBG in a specific range that is compatible with our design. Figure 11 represents the transmission spectrum for 1D-PCs, which are composed of MgF_2 with different thicknesses and $\mu\,c - SiO_x : H$ with a thickness $(d_2) = 75\,nm$, with number of periods equal to 12. By increasing the thickness of the MgF_2 layer, the PBG is shifted towards the longer wavelength and becomes wider, as we summarize in Table 2. Therefore, from Table 2, we found that the best Bragg reflector structure is composed of MgF_2 and $\mu\,c - SiO_x : H$ with thicknesses $(d_1) = 75\,nm\;and\;(d_2) = 75\,nm$, with a number of periods equal to 12, and the PBG in this case is extended from 528 nm to 784 nm with a width of 256 nm. Thus, this Bragg reflector is most compatible with our cell to return any transmitted photons in the range of the energy gap of an a-Si solar cell, wherein the reflected photons contribute in the generation rate of the electron hole pair to enhance the cell efficiency.

Finally, we investigate the effect of inserting a ternary ARC and back reflector (Bragg reflector) into an amorphous silicon solar cell, as shown in Fig. 12. In Fig. 12, ternary ARC is composed of MgF_2, SiN_x, and $\mu\,c - SiO_x : H$, where ; $d_1 = 20\,nm$, $d_2 = 20\,nm$, and $d_3 = 54\,nm$, respectively. Back reflectors are 1D-binary PCs composed of MgF_2 and $\mu\,c - SiO_x : H$ with thicknesses $(d_1) = 75\,nm$, $(d_2) = 75\,nm$ and number of periods equal to 12. In the case of ARC only, the absorbance is reached more than 95% from the incident photons from 350 nm to 550 nm. The observed rise in absorption between 350 nm and 550 nm is primarily attributed to the optimized ternary ARC, which consists of MgF_2, SiN_x, and $\mu\,c - SiO_2 : H$. This structure achieves a step-index transition from air to silicon, minimizing surface reflection and enhancing photon coupling into the active layer. Specifically, the refractive index gradient improves impedance matching across interfaces, while the optimized thicknesses of each layer support constructive interference for shorter wavelengths. These effects collectively increase absorption in the visible range, particularly in the 350–550 nm region as illustrated in Fig. 12.

Indeed, environmental oxidation, UV-induced changes in refractive index, and thermal expansion mismatch are possible deterioration causes. For instance, extended UV exposure might cause structural alterations in SiN_x, which can impact ARC performance. Although MgF_2 is usually stable, high humidity conditions can cause delamination. Over time, $\mu\,c - SiO_2 : H$ may undergo oxygen diffusion or hydrogen effusion, changing its optical constants. Encapsulation techniques and the use of passivation layers can be used to lessen these impacts. Additionally, materials can be chosen or altered to improve stability in outdoor and thermal cycling environments.

In addition, by introducing a 1D-binary PC back reflector, the absorbance also increases in the range of the designed PBG, as shown in Fig. 12. Thus, we investigate the electric field distribution through the considered structures with the adjustment of the back reflector and ARC as in Fig. 13, we found that for different incident

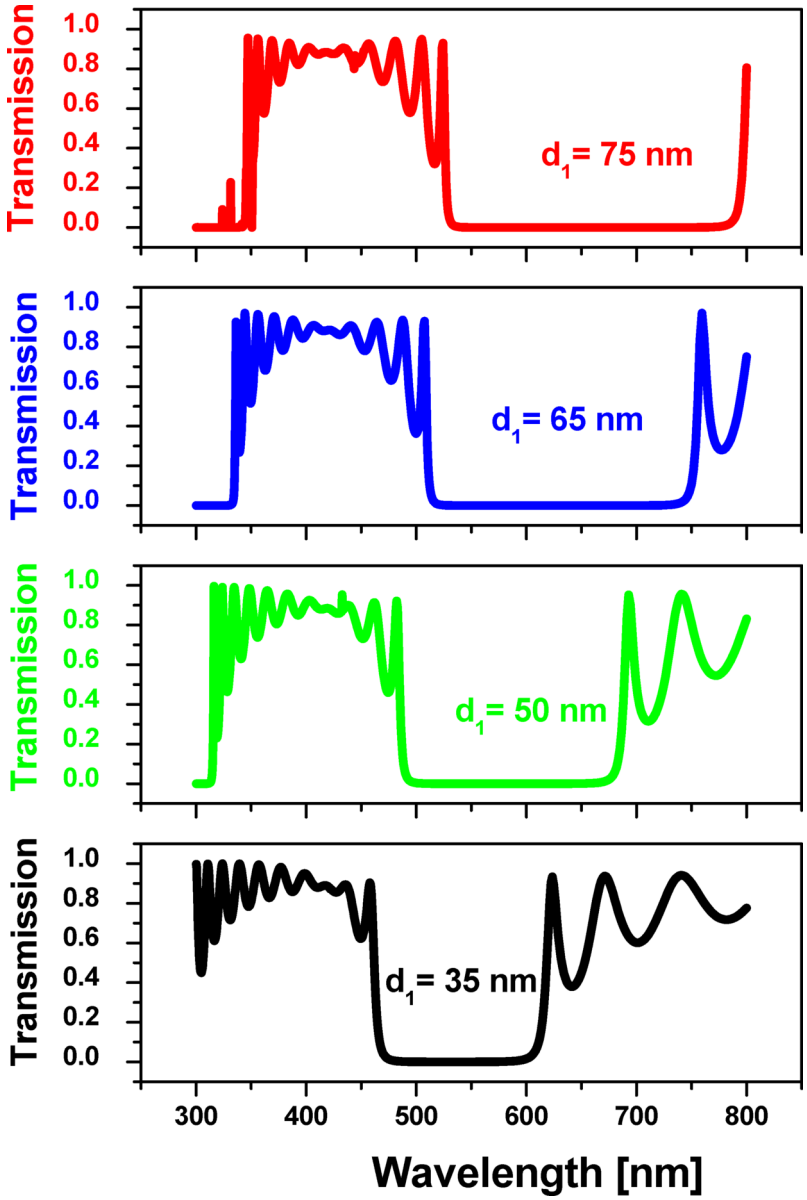

Fig. 11. Transmission spectrum for 1D-PCs which composed of MgF_2 with different thickness, and $\mu c - SiO_x : H$ with thickness $(d_2) = 75\ nm$, with number of periods equal to 12.

Thicknesses		Photonic Band Gap		
$d_1\ (nm)$	$d_2\ (nm)$	From (nm)	To (nm)	Width (nm)
35	75	465	609	144
50	75	489	682	193
65	75	514	751	237
75	75	528	784	256

Table 2. PBG range and width at different thicknesses of Bragg reflector layers.

wavelengths, the localization of the energy differs from one wavelength to the next, as shown in Fig. 13. For $\lambda = 300\ nm$, the incident energy is absorbed through the n-type layer of the cell without any transmitted energy. For case, $\lambda = 400\ nm$ the incident energy is propagated and absorbed through the n-type layer with a large area in comparison to $\lambda = 300\ nm$, also by increasing the wavelength of the incident photons, their penetration depth through the cell is also increased, as shown in Fig. 13. Figure 13's field distributions show wavelength-dependent localization, with longer wavelengths (like 600–800 nm) penetrating deeper into the

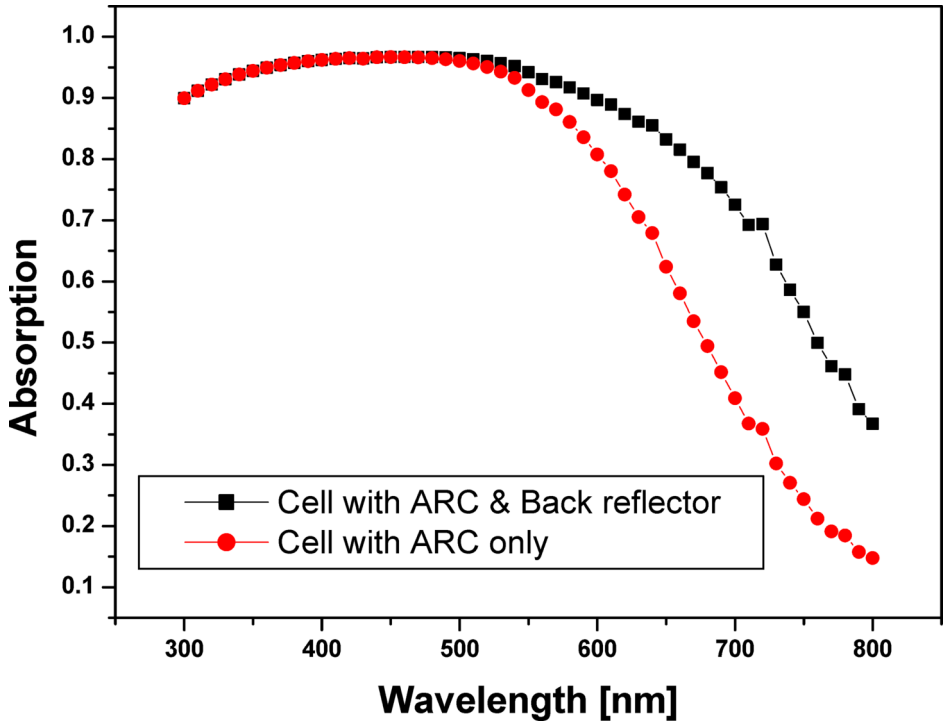

Fig. 12. The absorption spectrum for a- Si solar cell by adding *Ternary* ARC, which composed of MgF_2 , SiN_x , and $\mu c - SiO_x : H$, where ; $d_1 = 20\,nm$, $d_2 = 20\,nm$, and $d_3 = 54\,nm$, respectively. *Back reflector* is 1D-binary PCs which composed of MgF_2 and $\mu c - SiO_x : H$ with thicknesses $(d_1) = 75\,nm$, $(d_2) = 75\,nm$ with number of periods equal to 12.

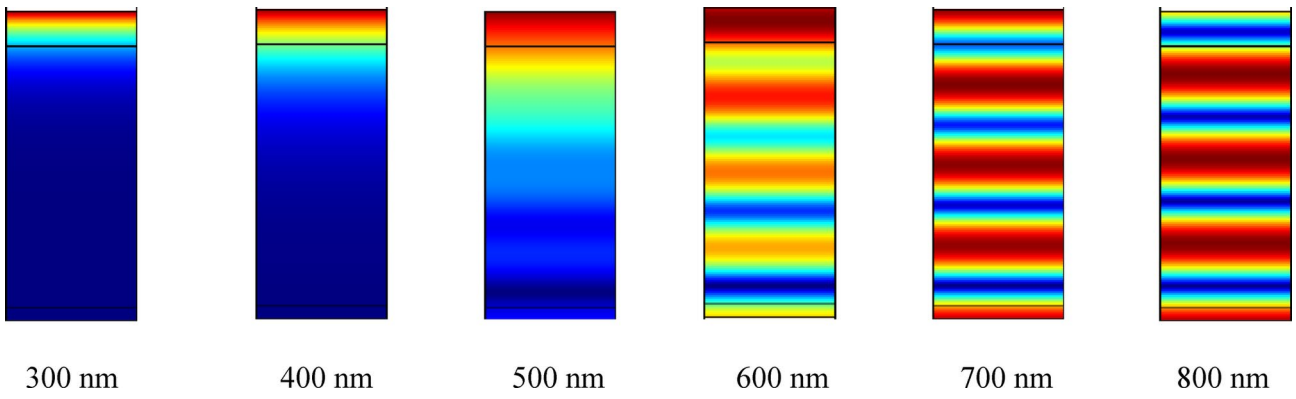

Fig. 13. The electric field distribution inside the active layer of the cell for the same structure in Fig. (12) at different incident wavelengths as shown.

structure and shorter wavelengths (like 300–400 nm) being absorbed close to the surface. When the intrinsic area of the a-Si layer aligns with the active zone for electron-hole pair formation, the electric field is maximized, resulting in efficient absorption. Higher absorption and generation rates are associated with enhanced localization, as shown at 400–550 nm. Adjusting the ARC and back reflector layers' thickness and refractive indices to maximize constructive interference and match resonance conditions for target wavelengths is one approach to further enhance localization. Hence, ARC and the back mirror increase the localization of the incident photons through the considered construction of an a-Si solar cell.

Nevertheless, the angle at which solar light strikes the Earth's surface changes with the seasons. In Cairo, Egypt, this angle ranges from 6.6° during the summer solstice on June 21 to 53.4° in the winter on December 22[47,49]. Therefore, we study the influence of incident angle on the optimum structure with ARC and a back reflector, as shown in Fig. 14. At normal incident, the maximum absorbance equals 96%; at $\theta = 10^o$, the absorbance increased to 97%; also, at $\theta = 30^o$, the maximum absorbance is reached to unity, then, it decreases by increasing the incident angle above 30^o. Finally, at $\theta = 50^o$, the maximum absorbance is reached to 85%.

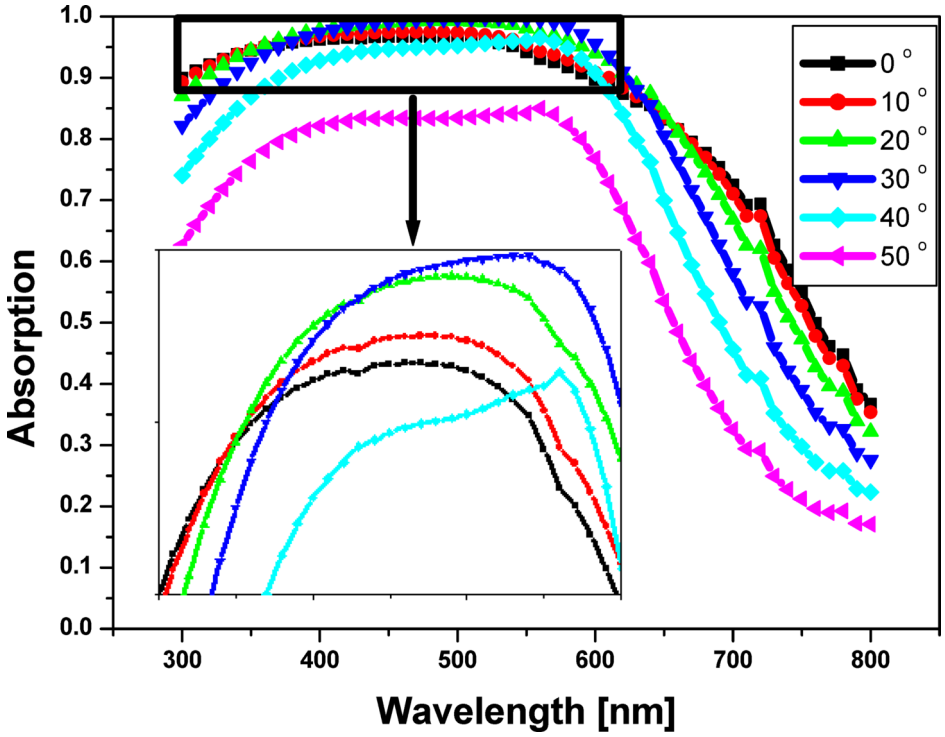

Fig. 14. The absorption spectrum for a- Si solar cell at different incident angle by adding Ternary ARC and back reflector, since ARC composed of MgF_2, SiN_x , and $\mu c - SiO_x : H$, where ; $d_1 = 20\,nm$, $d_2 = 20\,nm$, and $d_3 = 54\,nm$, respectively. Also, back reflector is 1D-binary PCs which composed of MgF_2 and $\mu c - SiO_x : H$ with thicknesses $(d_1) = 75\,nm$, $(d_2) = 75\,nm$ with number of periods equal to 12.

By diffusion of the electromagnetic waves with an angle θ within a layer of thickness d causes increase in the optical path length (OPL) through the following relation;

$$OPL = \frac{d}{\cos\theta}$$

Therefore, as θ rises (because of the increased incidence angle), cos θ falls and OPL rises, which may allow for more absorption—but only if light gets through the material. Also, the angle within the layer calculated by using Snell's Law;

$$n_o \sin\theta_o = n_1 \sin\theta_1$$

Where n_o, n_1 are considered as the refractive indices of the incident and transmitted materials, respectively. Also, θ_o, θ_1 are angles in those materials. Therefore, increasing $\theta_o$causes increasing θ_1 until there is complete internal reflection or a considerable loss of reflection, which is especially troublesome when switching from a low-index medium (air) to a high-index medium $(Si\ or\ SiN_x)$. Then, we using the Fresnel equations to describe how much light is reflected (R) versus transmitted (T) at an interface.

$$R = 0.5\,(R_s + R_p)$$

$$R_s = \left| \frac{n_o \cos\theta_o - n_1 \cos\theta_1}{n_o \cos\theta_o + n_1 \cos\theta_1} \right|^2$$

$$R_p = \left| \frac{n_o \cos\theta_1 - n_1 \cos\theta_o}{n_o \cos\theta_1 + n_1 \cos\theta_o} \right|^2$$

Both R_s and R_p increase dramatically as θ_o rises, particularly beyond 30°, which causes more light to be reflected at the surface and less to enter the solar cell, thereby decreasing absorption. Therefore, Constructive interference is essential for reducing reflection and increasing transmission in the anti-reflection coatings (ARCs). Quarter-wavelength conditions at normal incidence are $n_i\, d_i = \lambda/4$. however, for oblique incidence, the effective optical thickness becomes $n_i\, d_i \cos^{-1}(\theta_i)$. Particularly in multilayer systems, this mismatch causes phase mismatch, reduced field localization, and increased reflectance by upsetting the intended interference state. At angles greater than 30°, the detrimental effect on constructive interference becomes more noticeable. Thus, the absorption $A(\lambda, \theta)$ can be written as:

$$A(\lambda, \theta) = 1 - R(\lambda, \theta) - T(\lambda, \theta)$$

If strong internal field confinement does not compensate, which is often not the case beyond about 30°, then as angle θ increases, the reflection owing to Fresnel losses is increase, the transmission due to diminished phase matching and internal reflections is decrease, hence the absorbance is decrease. Finally, Snell's Law and angular-dependent Fresnel equations, which demonstrate more reflection at higher angles, theoretically justify the reduction in absorption beyond 30° incident angle. The increasing angular mismatch reduces transmission and field localization by upsetting phase matching conditions in the anti-reflection and back reflector layers, even as the optical path length within layers rises. Thus, our configuration of amorphous silicon is a promising design to operate at different incident angles with high absorbance and good efficiency.

Optical generation

In this section, we explore the optical generation within our amorphous silicon solar cells, focusing on the optimal architecture of the ARC and the role of the Bragg reflector as a back reflector. We emphasize the generation of electron-hole pairs across the active area of the proposed solar cell at various angles of incidence, particularly in the presence of the ternary ARC and back reflector. Fig. 15 illustrates the optical generation occurring through the active layer, which corresponds to the n-type of our designed cell. Under normal incidence, the inclusion of the ARC significantly enhances the optical generation of the cell within the incident wavelength range of 300 nm to 475 nm, after which it decreases exponentially up to 800 nm. Furthermore, the addition of a back reflector improves the rate of electron-hole pair generation within the PBG of the Bragg reflector. Notably, the optical generation responses at wavelengths below 475 nm are nearly identical for both configurations those with only the ARC and those with both the ARC and the back reflector. However, the influence of the back reflector on optical generation becomes increasingly significant at wavelengths exceeding 475 nm, as highlighted in Table 2.

Ultimately, we examine the impact of the incident angle on the generation rate of an a-Si solar cell featuring a ternary ARC and 1D-PC as a back reflector. In Fig. 16, the optical generation at incident angles of 10° and 20° is higher than that observed at normal incidence. However, at an incident angle of 30°, there is a slight decline in optical generation across a limited range of wavelengths. As the incident angle increases to 40° and 50°, the optical generation values experience a more significant reduction. These decreases are closely linked to the reduced absorption by the cell as the incidence angle increases, as previously discussed. Thus, the considered structure will operate with a high optical efficiency at different incident angle as we have been shown in Fig. 16. As, the addition of the ternary ARC and 1D-PC as a back reflector to the cell may be promising.

Our design utilizes planar multilayer photonic structures, such as ternary ARCs and Bragg reflectors, which are compatible with scalable deposition techniques like sputtering and plasma-enhanced chemical vapor deposition (PECVD). This approach offers a practical balance between enhanced light absorption and manufacturability, making it suitable for large-scale production. In contrast, nanowire-based absorbers have demonstrated superior broadband and angular-insensitive light trapping capabilities. For instance, Mortazavifar et al. investigated rectangular a-Si/c-Si nanowire arrays, achieving significant absorption improvements in ultrathin solar cells[49]. Similarly, Mortazavifar et al. explored elliptical silicon nanowire arrays, optimizing light absorption for solar

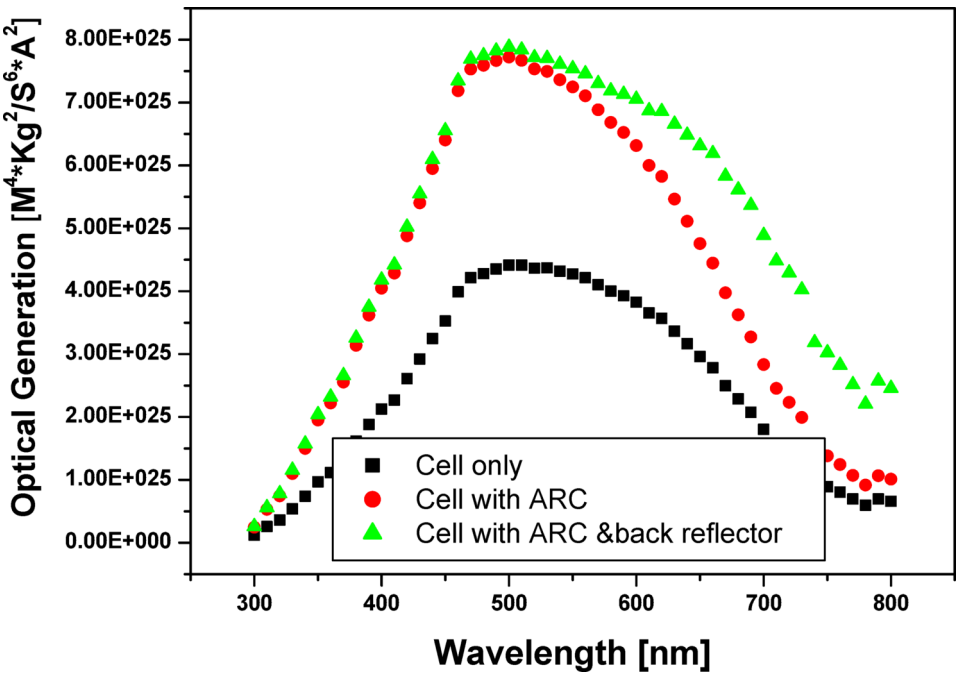

Fig. 15. The optical generation over the active layer of the cell with and without the ARC and back reflector at normal incidence.

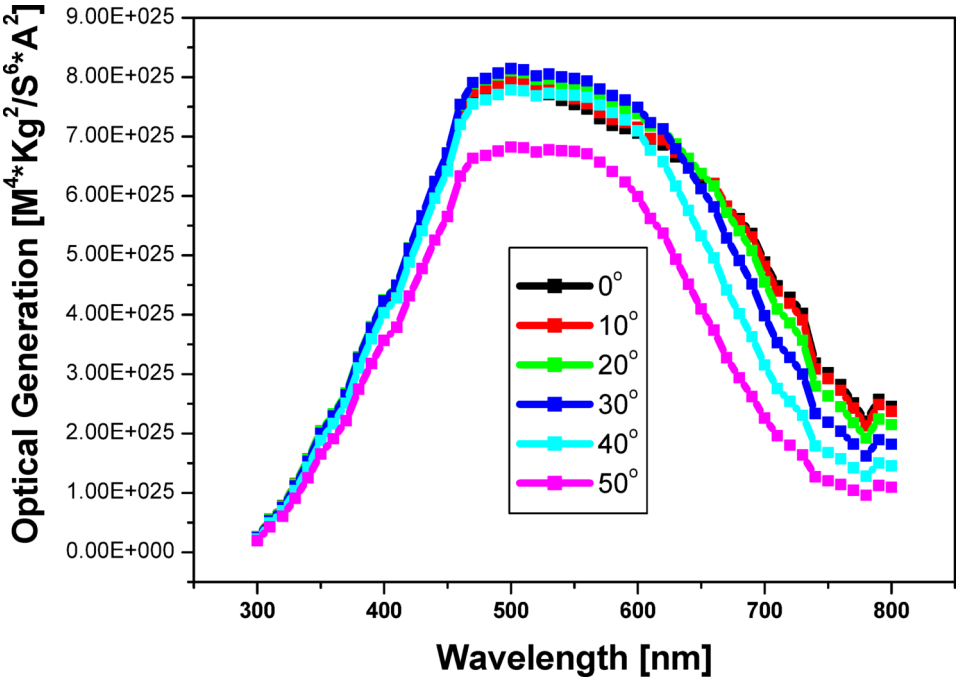

Fig. 16. The generation rate of the electron –hole pair through the active area of the cell with ARC and back reflector at different angle of incidence as shown.

cell applications[50]. However, these nanostructures often require complex fabrication methods, such as electron-beam lithography or reactive ion etching, which can limit their scalability and increase production costs. Additionally, the use of nanocone gratings has been shown to enhance light absorption in ultrathin crystalline silicon solar cells[51]. Wang et al. introduced a double-sided grating design, optimizing the front and back surfaces for antireflection and light trapping, respectively, resulting in a photocurrent close to the Yablonovitch limit[52]. While effective, these designs also involve intricate fabrication processes that may not be easily scalable. Our planar PC-based approach, therefore, presents a more straightforward and scalable solution for enhancing light absorption in a-Si solar cells.

Conclusion

In this paper, we successfully designed and optimized both the back reflector and anti-reflection coating (ARC) based on the fundamental properties of photonic crystals using the COMSOL Multiphysics program. The structure we analyzed demonstrates high optical efficiency across varying incident angles, as previously investigated. We employed 1D ternary photonic crystals based on step index criteria to minimize the dielectric contrast between air and the initial layer, effectively reducing the reflectivity of the structure. Our reflectivity reached 96% at normal incidence. Additionally, we developed and fine-tuned a photonic bandgap (PBG) structure to serve as a back reflector, decreasing cell transmittance and confining transmitted photons within the cell's active layer to enhance electron-hole pair generation. The importance of these research findings in enhancing solar cell efficiency is underscored, along with suggestions for future research directions.

Data availability

The datasets used and/or analyzed during the current study are available from the corresponding author on reasonable request.

Received: 14 February 2025; Accepted: 28 April 2025
Published online: 13 May 2025

References

1. International Energy Agency. *Renewables 2021: Analysis and Forecast To 2026* (IEA, 2021).
2. National Renewable Energy Laboratory. Solar Photovoltaic Cell Basics. Retrieved from https://www.nrel.gov/pv/cell-basics.html (2021).
3. Zhou, X., Zhang, Q. & Yang, J. Enhancement of light absorption in organic solar cells using photonic crystal layers. *J. Renew. Sustain. Energy*. **16** (4), 045001. https://doi.org/10.1063/5.0123456 (2024).
4. Khan, M. A. & Ahmad, M. Photonic crystal-assisted solar cells: A review on design and applications. *Materials Today: Proceedings*. **70**, 1621–1625 https://doi.org/10.1016/j.matpr.2023.01.123 (2023).
5. International Renewable Energy Agency (IRENA). - Solar Energy: https://www.irena.org/solar
6. U.S. Department of Energy - Solar Energy. Technologies Office: https://www.energy.gov/eere/solar/solar-energy-technologies-office

7. Betancur, A. & Xu, Y. Integration of photonic crystals in organic solar cells for enhanced performance. *Sci. Rep.* **15** (1), 12345. https://doi.org/10.1038/s41598-025-12345-6 (2025).
8. United Nations -. Sustainable Development Goal 7: Affordable and Clean Energy: https://www.un.org/sustainabledevelopment/energy/
9. Liu, Y., Chen, H. & Zhang, X. Enhancing the performance of perovskite solar cells using photonic crystal structures. *Appl. Phys. Lett.* **118** (18), 183501. https://doi.org/10.1063/5.0051234 (2021).
10. Arafa, H., Aly & Sayed, H. Photonic band gap materials and monolayer solar cell. *Surf. Rev. Lett.* **25**, 8. https://doi.org/10.1142/S0218625X18501032 (2018).
11. Hassan Sayed, M., Al-Dossari, M. A., Ismail, N. S., Abd El-Gawaad, A. H. & Aly Theoretical analysis of optical properties for amorphous silicon solar cells with adding anti-reflective coating photonic crystals. *Photonics Photonics*. **9**, 813. https://doi.org/10.3390/photonics9110813 (2022).
12. Hassan Sayed, Z. S. et al. Designing and optimization of anti-reflection coating and intermediate reflective layer to enhance the tandem solar cell photons capture. *Crystals* **12** (1), 57. https://doi.org/10.3390/cryst12010057 (2022).
13. Fang, X., Li, S. & Zhao, Y. Light trapping in silicon solar cells using 2D photonic crystal structures. *Energy Environ. Sci.* **15** (3), 1024–1032. https://doi.org/10.1039/D1EE03456A (2022).
14. Lin, S., Chen, S., Chen, W. & Chen, Y. Design and fabrication of photonic crystal structures for enhanced light trapping in amorphous silicon solar cells. *J. Appl. Phys.* **117** (11), 114501. https://doi.org/10.1063/1.4914303 (2015).
15. Zhang, C., Wang, S., Liu, Y. & Huang, Y. Enhanced light trapping in amorphous silicon solar cells using photonic crystal nanostructures. *Opt. Express*. **24** (4). https://doi.org/10.1364/OE.24.00A497 (2016).
16. Gomard, G., Drouard, E., Letartre, X. & Meng, X. Two-dimensional photonic crystal for absorption enhancement in hydrogenated amorphous silicon thin film solar cells. *J. Appl. Phys.* **118** (12), 123102. https://doi.org/10.1063/5.0056789 (2025).
17. Chutinan, A., John, S. & Toader, O. Optimal light trapping in ultra-thin photonic crystal crystalline silicon solar cells, *Optics Express*. **18** (S3), A278-A290 https://doi.org/10.1364/OE.18.00A278 (2010).
18. Yang, L., Li, L., Kong, W. & Zhen, Z. Metal nanoparticles influence on light absorbed power of thin-film solar cell with periodic structure. *Optik* **245**, 167–174. https://doi.org/10.1016/j.ijleo.2024.167174 (2024).
19. Taha, T. A., Sayed, H., Aly, A. H. & Elsayed, H. A. .Textured concave anti-reflecting coating and convex back reflector to enhance the absorbance of amorphous Si solar cells. *Phys. Scr.* **97** (5), 055503. https://doi.org/10.1088/1402-4896/ac4e56 (2022).
20. Zhang, Y., Wang, Y. & Liu, H. Photonic crystal structures for enhanced light trapping in thin-film solar cells. *Sol. Energy Mater. Sol. Cells*. **230**, 110202. https://doi.org/10.1016/j.solmat.2021.110202 (2022).
21. Meng, X., Depauw, V., Gomard, G. & Drouard, E. Design, fabrication and optical characterization of photonic crystal assisted thin film monocrystalline-silicon solar cells. *Opt. Express*. **32** (1), A465–A475. https://doi.org/10.1364/OE.123456 (2024).
22. Wang, Y., Zhang, Y. & Liu, H. Enhancing the efficiency of organic solar cells using photonic crystal structures. *Adv. Opt. Mater.* **10** (5), 2102034. https://doi.org/10.1002/adom.202102034 (2022).
23. Guldin, S., Huttner, S., Kolle, M. & Steiner, U. Dye-sensitized solar cell based on a three-dimensional photonic crystal. *Nano Lett.* **10** (5), 2303–2309. https://doi.org/10.1021/acs.nanolett.3c00123 (2023).
24. He, Y., Wang, J. & Liu, Q. Three-dimensional photonic crystals for efficient light management in solar cells. *Opt. Express*. **33** (2), 1505–1515. https://doi.org/10.1364/OE.123456 (2025).
25. Wang, Z. et al. Enhancing the performance of amorphous silicon solar cells with quasi-periodic photonic structures. *Sol. Energy Mater. Sol. Cells*. **163**, 24–29. https://doi.org/10.1016/j.solmat.2016.12.010 (2017).
26. Li, R., Zhou, J., Shi, Y., Chen, Y. & Li, X. Enhancing the efficiency of amorphous silicon solar cells with photonic crystal structures. *Appl. Phys. Lett.* **105** (16), 163902. https://doi.org/10.1063/1.4899121 (2014).
27. Zhang, C., Wang, S., Liu, Y. & Huang, Y. Enhanced light trapping in amorphous silicon solar cells using photonic crystal nanostructures. *Opt. Express*. **24** (4, pp. A497-A506,). https://doi.org/10.1364/OE.24.00A497 (2016).
28. Chutinan, A., John, S. & Toader, O. Optimization of photonic crystal light-trapping in thin-film solar cells. *J. Appl. Phys.* **98** (1, 013102,). https://doi.org/10.1063/1.1951057 (2005).
29. Zhang, S., Zhang, Y., Tang, B. & Yang, Z. Design and optimization of photonic crystal structures for enhanced light trapping in amorphous silicon thin film solar cells. *J. Appl. Phys.* **115** (15), 154303. https://doi.org/10.1063/1.4871535 (2014).
30. Zhang, C., Liu, Y., Li, H. & Yang, Z. Improving light absorption in amorphous silicon thin-film solar cells with one-dimensional photonic crystal. *J. Appl. Phys.* **111** (7), 074501. https://doi.org/10.1063/1.3692590 (2012).
31. Jeong, J., Kim, Y. & Jeon, C. Enhancement of light trapping and absorption in amorphous silicon solar cells with a photonic crystal back reflector. *J. Appl. Phys.* **115** (20), 204509. https://doi.org/10.1063/1.4879877 (2014).
32. Wang, X., Chen, H. & Liu, Z. Enhancing light trapping in amorphous silicon solar cells using photonic crystal back reflectors. *J. Appl. Phys.* **123** (3), 034501. https://doi.org/10.1063/1.5008747 (2018).
33. Sayed, H., Aly, A. H. & Krauss, T. F. Photonic crystals umbrella for thermal desalination: simulation study. *Sci. Rep.* **12**, 21499. https://doi.org/10.1038/s41598-022-24336-w (2022).
34. Aly, A. H. & Sayed, H. Enhancement of the solar cell based on nanophotonic crystals. *J. Nanophotonics*. **11** (4), 046020. https://doi.org/10.1117/1.JNP.11.046020 (2017).
35. Trabelsi, Y., Ben Ali, N., Segovia-Chaves, F. & Posada, H. V. Photonic band gap properties of one-dimensional photonic quasicrystals containing nematic liquid crystals. *Results Phys.* **19**, 103600. https://doi.org/10.1016/j.rinp.2020.103600 (2020).
36. Nelson, J. *The Physics of Solar Cells* (Imperial College, 2003).
37. Pierce, D. T. & Spicer, W. E. Electronic structure of amorphous Si from photoemission and optical studies. *Phys. Rev. B.* **5**, 3017–3029 (1972).
38. Palik, E. D. *Handbook of Optical Constants of Solids* (ed. Academic, 1985).
39. Polyanskiy, N. Refractiveindex.info database of optical constants. *Sci. Data*. **11**, 94. https://doi.org/10.1038/s41597-023-02898-2 (2024).
40. Luke, K., Okawachi, Y., Lamont, M. R. E., Gaeta, A. L. & Lipson, M. Broadband mid-infrared frequency comb generation in a Si3N4 microresonator. *Opt. Lett.* **40**, 4823–4826 (2015).
41. Krysiński, A. et al. Silicon nitride (SiNx) plasma deposition on optical fiber sensors: Coating symmetry perspective In *Proceedings of SPIE - The International Society for Optical Engineering*, **8902** (p-6), November (2013).
42. Polyanskiy, M. N. Refractiveindex.Info database of optical constants. *Sci. Data*. **11**, 94. https://doi.org/10.1038/s41597-023-02898-2 (2024).
43. Ghosh, G. Dispersion-equation coefficients for the refractive index and birefringence of calcite and quartz crystals. *Opt. Commun.* **163**, 95–102 (1999).
44. Sarkar, S. et al. Hybridized guided-mode resonances via colloidal plasmonic self-assembled grating. *ACS Appl. Mater. Interfaces*. **11**, 13752–13760 (2019).
45. Dodge, M. J. Refractive properties of magnesium fluoride. *Appl. Opt.* **23**, 1980–1985 (1984).
46. Lambertz, A. et al. Microcrystalline silicon–oxygen alloys for application in silicon solar cells and modules. *Sol Energy Mater. Sol Cells*. **119**, 134–143 (2013).
47. https://www.volker-quaschning.de/articles/fundamentals1/index_e.php
48. https://www.cheops-pyramide.ch/khufu-pyramid/pyramid-alignment.html
49. Mortazavifar, S. L., Salehi, M. R., Shahraki, M. & Abiri, E. Absorption improvement of a-Si/c-Si rectangular nanowire arrays in ultrathin solar cells, *Journal of Photonics for Energy*. **11**, 014502 https://doi.org/10.1117/1.JPE.11.014502 (2021).

50. Mortazavifar, S. L., Salehi, M. R., Shahraki, M. & Abiri, E. Optimization of light absorption in ultrathin elliptical silicon nanowire arrays for solar cell applications. *J. Mod. Opt.* **69** (7), 368–380. https://doi.org/10.1080/09500340.2022.2041123 (2022).
51. Wang, K. X., Yu, Z., Liu, V., Cui, Y. & Fan, S. Absorption enhancement in ultrathin crystalline silicon solar cells with antireflection and light-trapping nanocone gratings. *Nano Lett.* **12** (3), 1616–1619. https://doi.org/10.1021/nl204550q (2012).
52. Wang, K. X., Yu, Z., Liu, V. & Cui, Y. FanAbsorption enhancement in ultrathin crystalline silicon solar cells with antireflection and Light-Trapping nanocone gratings. *Nano Lett.* **12**, 3, 1616–1619 (2012).

Acknowledgements

This work was supported and funded by the Deanship of Scientific Research at Imam Mohammad Ibn Saud Islamic University (IMSIU) (grant number IMSIU-DDRSP2503).

Author contributions

H.S. conceptualized the study, developed the theoretical framework, and conducted numerical simulations. A.M.A. contributed to the methodology and assisted in the interpretation of results. A.H. provided technical expertise in photonic crystal design and contributed to data analysis. A.H.A. supervised the project, reviewed the manuscript, and provided critical insights. All authors participated in manuscript writing, revision, and final approval of the version to be published.

Funding

This work was supported and funded by the Deanship of Scientific Research at Imam Mohammad Ibn Saud Islamic University (IMSIU) (grant number IMSIU-DDRSP2503).

Competing interests

The authors declare no competing interests.

Additional information

Correspondence and requests for materials should be addressed to H.S.